GENERATION OF NON-ROCKING TRAVELING WAVE BY FINITE ELEMENT ANALYSIS AT CYLINDRICAL STATOR OF PIEZOELECTRIC MICROMOTOR

Mohammad Ahsan Ullah[(1)] and Fatematuz Zohora[(2)]

[1]Department of Mechanical Engineering, Bangladesh University of Engineering & Technology (BUET)
[2]Department of Mechanical Engineering, Military Institute of Science & Technology (MIST)

Abstract:
In this paper, a vibration mode shape of multiple wavelengths of a cylinder is searched with the aim of generating a non-rocking traveling wave at the end face of a cylindrical stator. The finite element analysis (FEA) results reveals that a 3λ mode shape can be realized with a short aluminum cylinder of 14 mm in OD, 12 mm in ID, and 10 mm in length at a frequency of 121 kHz. A stator is modeled by trimming the outer face of the cylinder to twelve flat faces and bonding twelve piezoelectric PZN-PT single crystals as active element with a dimension of 10 mmL × 2.72 mmW × 0.5 mmT (P). The crystals are arranged into two sets consisting six crystals each such that the desired 3λ mode shape is realized when either set of crystals is excited with a sinusoidal voltage signal. When both sets of crystals are excited simultaneously with two sinusoidal ac voltage signals with 90° phase difference, a traveling wave of the 3λ mode shape is generated. The axial displacement of the traveling wave is found ±84 nm at a voltage of ±20V.

Keywords: *traveling wave, finite element analysis (FEA), piezoelectric, PZN-PT, frequency.*

1.0 INTRODUCTION:

The study of piezoelectric micromotors has become a center of attraction for their simple structure, high torque and low speed characteristics. Existing cylindrical piezoelectric micromotors are driven by bending vibration of the stator [1]-[9]. This bending vibration has only one crest and one trough or one-λ mode shape at the end face of the cylindrical stator, λ being the wave length. This one-λ mode shape is utilized in cylindrical piezoelectric micromotor developed by Dhong et al. [1], Kanda et al. [2], Koc et al. [3], Kurosawa et al. [4], and Morita et al. [5]-[9].

Using a titanium cylinder of 10 mm long, 2.4 mm OD, and 0.25 mm thick Marita et al. found one-λ mode at 106 kHz as shown in Figure 1(b). Utilizing this one-λ bending vibration mode one wavelength traveling wave is generated that consists only one crest and one trough around the cylinder end face as shown Figure 1(c).

For this one-wavelength traveling wave, a rotor cap placed onto of it is in contact with the cylinder end at only one point. The traveling wave generated from this vibration mode is thus not a "stable" configuration in that the axis of the cylinder not fixed at a point but moving along a circular locus when viewed from the top, causing it to "rock" as a result.

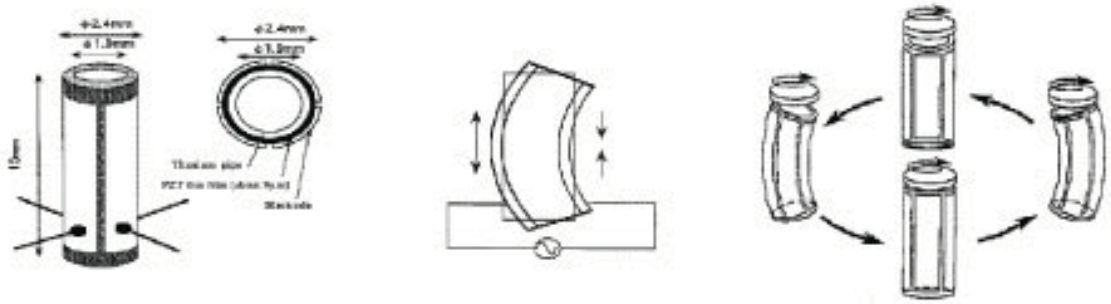

(a) (b) (c)

Fig 1: (a) Stator structure (b) Excitation of bending vibration (c) One wavelength traveling wave generation of Marita et al. micromotor [5]

The objective of this paper is to design a cylindrical stator that is capable of generating traveling wave of multiple wavelengths at their end faces to eliminate the rocking of one wavelength traveling wave. Generation of traveling wave is shown by finite element analysis.

2.0 DESCRIPTION :

To generate multi wavelength traveling wave, a mode shape of a cylinder is needed to determine first that consists more than one crest at the end face.

2.1 Finite element analysis of free vibration of cylinder:

Mode shape and corresponding natural frequency of a vibrating cylindrical body is studied by means of Finite Element Analysis (FEA) using ABAQUS software. One-crest bending vibration mode shown in Figure 2 is found at 175 kHz for an aluminum cylinder of 3 mm in outer diameter, 2 mm in inner diameter, and 8 mm in length. The properties of the cylinder material used in the simulation are given in Table 1. ABAQUS / Standard element C3D20R is used in the simulation which is a 20-node quadratic brick reduced integration element. The boundary condition was encastre of a node where U1 = U2 = U3 = UR1 = UR2 = UR3 = 0. This boundary condition removes the rigid body motion.

Table 1: Properties of aluminum

Property	Value
Young's Modulus, E (GPa)	68
Poisson ratio, μ	0.35
Density (kg/m^3)	2,700

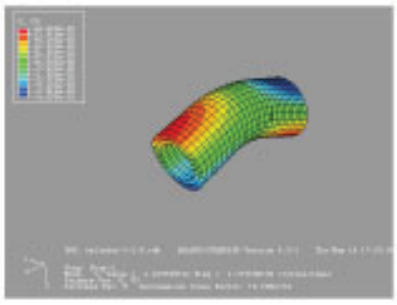

Fig2: One-crest bending mode at 175 kHz for a cylinder of 3mm in OD, 2mm in ID, and 8mm in length

Our interest is to generate clear mode shapes with two-crest, three-crest, and four-crest at each end of the cylinder with resonance frequencies of <200 kHz. Preliminary FEM results obtained revealed that suitable cylinder geometry is that having 14 mm in outer diameter, 12 mm in inner diameter, and 10 mm in length. For this cylinder size and properties of Table 1, two-crest mode shape (or 2λ or two wavelength mode shape) is found at 117 kHz, three-crest mode shape (or 3λ or three wavelength mode shape) is found at 121 kHz, and four-crest mode shape (or 4λ or four wavelength mode shape) is found at 146 kHz. These mode shapes are shown in Figure 3.

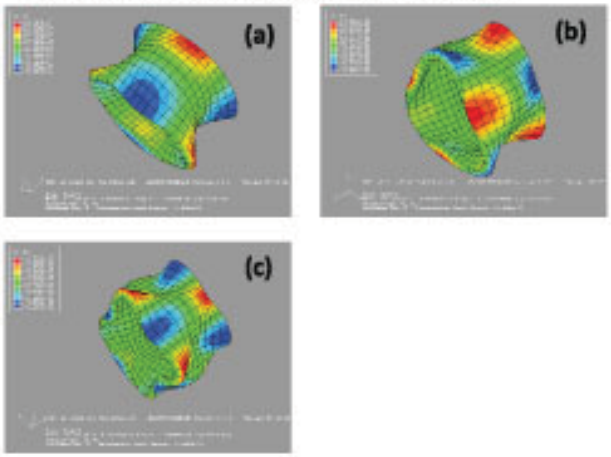

Fig 3: (a) Two-crest (b) three-crest and (c) four-crest mode shape for a cylinder of 14 mm in OD, 12 mm in ID, and 10 mm in length.

2.2 Vibration mode of choice for non-rocking traveling wave:

One-crest bending mode (one-wavelength or 1λ mode) of a cylinder has been used in actuators by many researchers to drive cylindrical micromotor. A rotor is pressed against the end face of the cylinder. When a traveling wave of bending mode is generated around the circumference of the cylinder end face, a frictional force is created between the rotor and the crest of bending mode. Hence, frictional force is transferred to rotor through one point (crest) only. It creates rocking or unsteady rotation of rotor.

If the number of crests is increased around the cylinder end face, this rocking rotation will be reduced. To minimize the rocking rotation, two-crest, three-crest, and four-crest mode shape are preferred over 1-crest mode. However,

when the number of crest or wavelength (λ) is increased, the amplitude of vibration decreased accordingly.

Considering that (i) non-rocking rotation $\propto\lambda$ or number of crest, and (ii) amplitude of vibration $\propto \frac{1}{\lambda}$ quality and vibration amplitudes of 2-crest, 3-crest, and 4-crest mode shape cylindrical vibrators.

Table 2: Comparison of traveling wave generation ability, vibration amplitude and non-rocking quality of different vibration modes of cylinder

Mode shape	Crest position around cylinder end face	Resonance frequency	Vibration amplitude	Traveling wave generation	Stability of cylinder axis when vibrate
1λ-mode (1-crest)	One crest only	-	Largest	Possible	Rocking
2λ-mode (2-crest)	Crests are 180° away with each other in 360°	117 kHz	High intermediate	Possible	Rocking remains possible
3λ-mode (3-crest)	Crests are 120° away with each other in 360°	121 kHz	Low intermediate	Possible	Stable (non-rocking)
4λ-mode (4-crest)	Crests are 90° away with each other in 360°	146 kHz	Lowest	Possible	Stable (non-rocking)

From Table 2, it is seen that the crests lays 180° away with each other in 2-crest mode shape. This indicates a chance of rocking rotation remains. Hence, two-crest mode shape can be discarded. While four-crest and higher modes produce stable traveling wave, their vibration amplitude decrease accordingly with the degree of mode shape. For this reason, three-crest mode shape is chosen for our further study as it provides large-amplitude, non-rocking traveling wave.

2.3 ELABORATION OF THE CHOSEN MODE SHAPE:

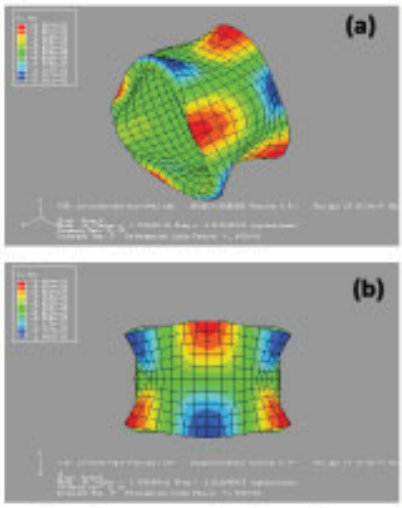

Fig 4: The chosen mode shape for non-rocking traveling wave (a) isometric view (b) side view.

Fig 4: The chosen mode shape for non-rocking traveling wave (a) isometric view (b) side view.

The chosen mode shape is again shown in Figure 4 for further elaboration purpose. The red colors indicate the displacement in the positive axial direction, and the blue colors indicate the displacement in the negative axial direction. The figure shows that the mode shape has six strain sections at each end. Three of them extend in the axial direction while the other three contracts. The figure further shows that the opposite ends of a stressed section extend or contract simultaneously in the axial direction. That is, in this vibration mode, there are three crests and three troughs along the entire circumference of the end face of the cylinder.

2.4 Modeling of the Cylindrical Stator:

The dimensions of the cylinder chosen are 14 mm in outer diameter, 12 mm in inner diameter, and 10 mm in length. The outer surface of the cylinder is trimmed to twelve flat faces as shown in Figure 5(a) while its inner surface remains circular.

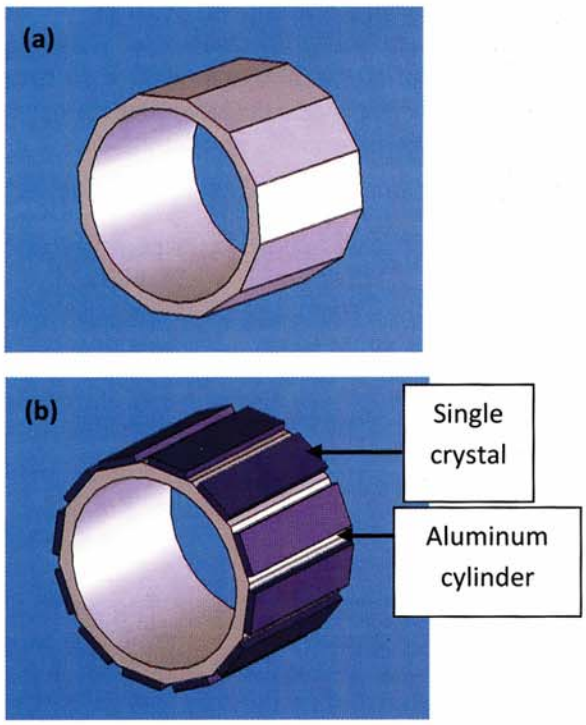

Fig 5: (a) Twelve flat faces cylinder (b) Twelve single crystal plate bonded cylinder.

Twelve single crystal active elements are bonded onto the outer surface of the cylinder, one at each side face as shown in Figure 5(b). The crystals are arranged into two sets, each consisting of six crystals spaced at 60° apart. The two sets of crystals are offset by 30° with respect to one another, such that the crystals from each set are spaced by a crystal from the other set.

In this work, relaxor based piezoelectric PZN-PT single crystals are used as the active elements because of their superior electromechanical properties compared to state-of-the-art PZT piezoceramics. The cut and dimensions of the single crystals used (P indicates poling direction) are as follows:

Crystal cut: $[110]^L \times [1\text{-}10]^W \times [001]^T$ (P) ; L being the active direction

Crystal dimensions: 10 mm^L × 2.72 mm^W× 0.5 mm^T (P)

Crystal density = 8300 kg/m^3

The piezoelectric and stiffness matrices of the above crystal cut have been determined by Shukla et al. [10]. They are given below for easy reference. Note that this crystal cut has a 4mm symmetry with $d_{31} = d_{32}$, $C_{11} = C_{22}$, $C_{31} = C_{32}$ and $C_{31} = C_{55}$.

Piezoelectric constant matrix,

$$\begin{bmatrix} 0 & 0 & 0 & 0 & d_{15} & 0 \\ 0 & 0 & 0 & d_{24} & 0 & 0 \\ d_{31} & d_{32} & d_{33} & 0 & 0 & 0 \end{bmatrix} = \begin{bmatrix} 0 & 0 & 0 & 0 & 550 & 0 \\ 0 & 0 & 0 & 550 & 0 & 0 \\ -1537 & -1537 & 3087 & 0 & 0 & 0 \end{bmatrix} \times 10^{-12}\ C/N$$

Stiffness matrix,

$$\begin{bmatrix} C_{11} & C_{12} & C_{13} & 0 & 0 & 0 \\ C_{21} & C_{22} & C_{23} & 0 & 0 & 0 \\ C_{31} & C_{32} & C_{33} & 0 & 0 & 0 \\ 0 & 0 & 0 & C_{44} & 0 & 0 \\ 0 & 0 & 0 & 0 & C_{55} & 0 \\ 0 & 0 & 0 & 0 & 0 & C_{66} \end{bmatrix}^E = \begin{bmatrix} 163 & 34 & 95 & 0 & 0 & 0 \\ 34 & 163 & 95 & 0 & 0 & 0 \\ 95 & 95 & 101 & 0 & 0 & 0 \\ 0 & 0 & 0 & 64 & 0 & 0 \\ 0 & 0 & 0 & 0 & 64 & 0 \\ 0 & 0 & 0 & 0 & 0 & 29 \end{bmatrix}^E \times 10^9\ N/m^2$$

2.5 Forced Vibration of Cylinder with PZT Single Crystal:

Finite element analysis has been done to determine the mode shape of the cylinder excited by piezoelectric single crystals. Perfect bonding between the single crystal and the cylinder is assumed in the simulation.

The meshing of model is shown in Figure 6. In the meshing, hexahedral elements have been used for both the aluminum cylinder and the piezoelectric single crystals. C3D20R is used for aluminum cylinder which is a 20-node quadratic brick reduced integration element and C3D20RE is used for piezoelectric material which is a 20-node quadratic piezoelectric brick reduced integration element. To remove the rigid body motion both mechanical and electrical boundary condition was applied. Mechanical boundary condition was encastre of a node of aluminum cylinder where U1 = U2 = U3 = UR1 = UR2 = UR3 = 0. Electrical boundary condition for piezoelectric material was electrical potential of a node is zero. Our computer simulation results show that under the condition of free vibration, the assembled vibrator exhibits a similar mode shape of 3 crests and 3 troughs as in Figure 4 but at a slightly lower natural frequency of 88 kHz, probably a result of the added mass of the single crystals. An a.c. voltage signal of 88 kHz is thus applied to individual single crystals to excite the cylinder to vibrate at resonance in our subsequent simulation.

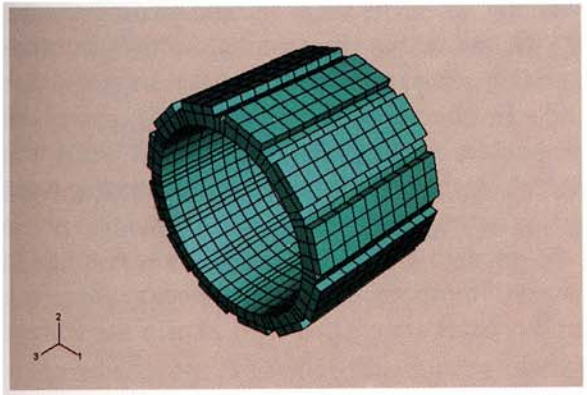

Fig 6: The meshing of the model

To generate the mode shape of 3-crests and 3-troughs, six alternate crystals are excited by a sinusoidal a.c. voltage at 88 kHz as shown in Figure 7. Of the six crystals, three are subjected to a voltage with 0° phase angle, i.e., +sin(ωt), and the other three of 180° phase angle, i.e., −sin (ωt), as shown in the figure.

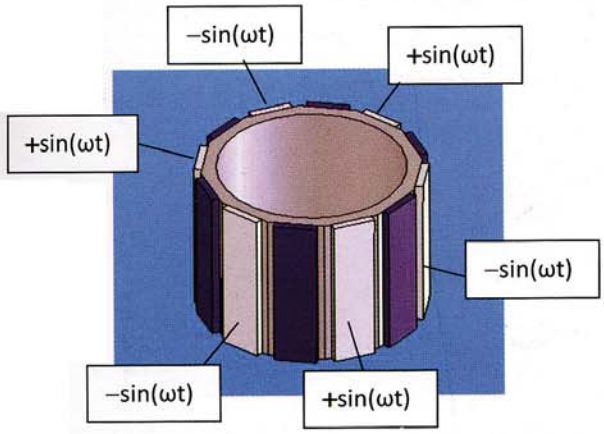

Fig 7: Applied electrical signals to the crystals to generate the desired mode shape

Figure 8 shows the mode shape of the cylinder when the crystals are excited by an a.c. voltage of 20 V at 88 kHz. The mode shape produced corresponds to 3λ mode shape (i.e. 3-crests and 3-troughs) at each end as per design. When the phase angle of the driving voltage is changed to 180°, the same mode shape is again observed but the crests now become the troughs and vice versus, as shown in Figure 8(b). Thus, for the electrical loading shown in Figure 7, a standing wave is generated at the both ends of the cylinder having six antinodes (3-crests, and 3-troughs) and six nodes.

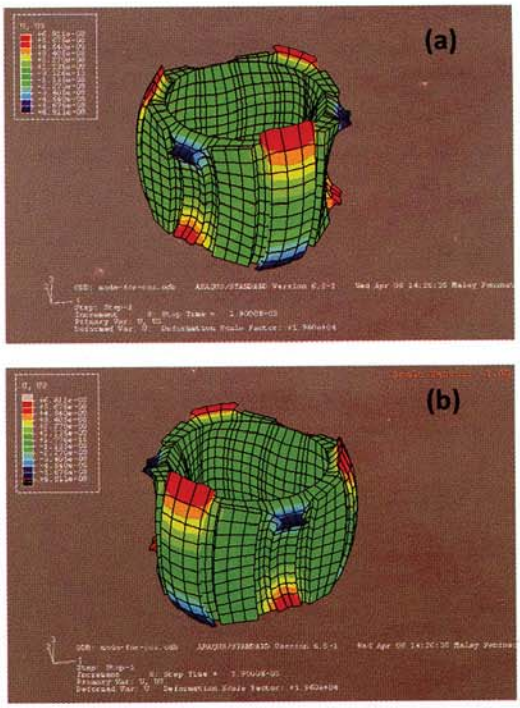

Fig 8: The mode shape at (a) 0° phase angle (b) 180° phase angle

2.6 Generation of the Traveling Wave:

The mode shape described above is that of standing wave. Attempts are then made to simulate the generation of a traveling wave in the vibrator by means of the finite element modeling. To achieve this, two standing waves are generated simultaneously whose phases are different by 90°, both spatially and temporally.

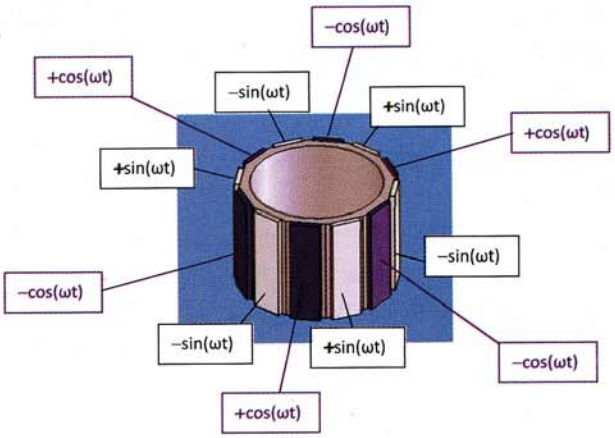

Fig 9: Applied electrical signals to the crystals to generate the traveling wave

Figure 9 shows the applied electrical signals to the crystals to generate the traveling wave. When the set of six white-colored crystals are excited with a sinusoidal ac voltage a standing wave is generated as shown in Figure 8. This standing wave has six antinodes and six nodes. All antinodes lie along the white-colored crystals and all nodes lie along the blue-colored crystals of Figure 9. This means, the spatial phase difference between consecutive white- and blue-colored crystals is quarter wave length or 90° (i.e., consecutive node and antinodes always have quarter wave length or 90° phase difference).

Similarly, when the set of six blue-colored crystals are excited with a sinusoidal ac voltage, another standing wave is generated with six antinodes and six nodes, all antinodes lying along the blue-colored crystals and all nodes along the white-colored crystals. Hence, this standing wave has quarter wave length or 90° spatial phase difference to the previously described case. To have 90° temporal phase difference, the blue-colored crystals are excited with a cosine ac voltage signal.

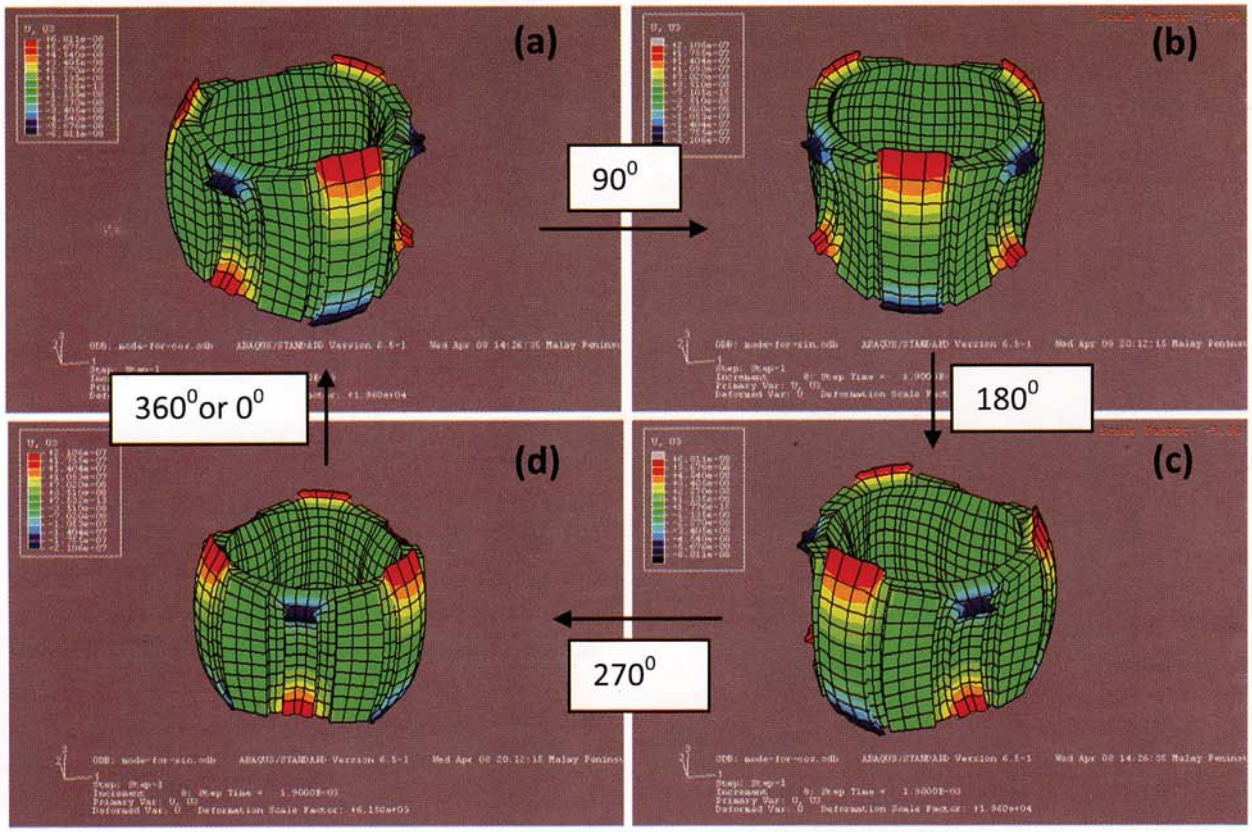

Fig 10: Generation of the traveling wave by superimposing two standing waves differing by 90° both spatially and temporally.

When the above two standing waves, which differ by 90° both spatially and temporally, are superimposed, a traveling wave results. Our simulation results also confirm that this is indeed the case, as shown in Figure 10.

The axial displacement of the traveling wave is found ±84 nm at a voltage of ±20V as shown in Figure 11, giving a displacement of 4.2 nm per volt.

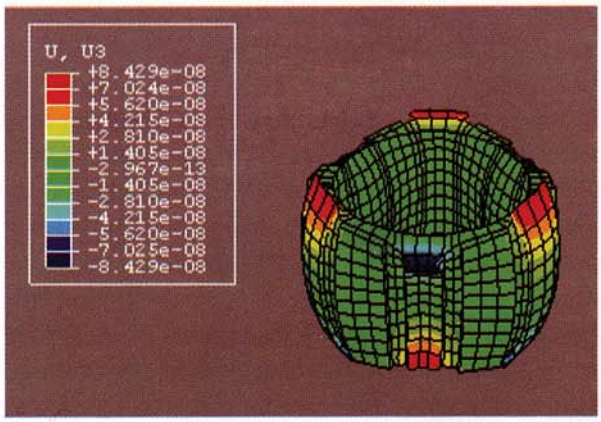

Fig 11: Axial displacement

3.0 CONCLUSION:

Extensive finite element analysis is carried out initially in search for a suitable vibration mode for a cylinder to generate non-rocking traveling wave at the end face of the cylinder. A bending vibration mode with 3-crests and 3-troughs (or 3λ) is found for an aluminum cylinder of 14 mm in OD, 12 mm in ID, and 10 mm in length which shows good potential for further study.

In the subsequent simulation, the outside surface of the cylinder is trimmed to twelve flat surfaces to accommodate twelve PZN-PT piezoelectric single crystal active elements. The crystals are arranged into two sets consisting six crystals each such that the desired 3λ mode shape is realized when either set of crystals is excited with a sinusoidal voltage signal. When both sets of crystals are excited with two sinusoidal ac voltage signals with 90° phase difference, a traveling wave of the 3λ mode shape is generated. The axial displacement of the traveling wave is found ±84 nm at a voltage of ±20V.

References:

[1] Dhong S., Lim S. P., Lee K. H., Zhang J., Lim L. C., and Uchino K., 2003. Piezoelectric ultrasonic micromotor with 1.5 mm diameter, IEE transaction on ultrasonics, ferroelectrics and frequency control, Volume 50, No. 4, pp. 361-367

[2] Kanda T., Makino A., Ona T., Suzumori K., Morita T., and Kurosawa M. K., 2006. A micro ultrasonic motor using a micro-machined cylindrical bulk PZT transducer, Sensors and actuators A, Elsevier, Volume 127, pp. 131-138.

[3] Koc B., Cagatay S., and Uchino K., 2003. A piezoelectric motor using two orthogonal bending modes of a hollow cylinder, IEE transaction on ultrasonics, ferroelectrics and frequency control, Volume 49, No. 4, pp. 495-500.

[4] Kurosawa M. K., Nakamura K., Okamoto T., and Ueha S., 1989. An ultrasonic motor using bending vibrations of a short cylinder, IEE transaction on ultrasonics, ferroelectrics and frequency control, Volume 36, No. 5, pp. 517-521

[5] Morita T., Kurosawa M. K., and Higuchi T., 2000. A cylindrical shaped micro ultrasonic motor utilizing PZT thin film (1.4 mm in diameter and 5.0 mm long stator transducer), Sensors and actuators A, Elsevier, Volume 83, pp. 225-230.

[6] Morita T., Kurosawa M. K., and Higuchi T., 1999. Cylindrical micro ultrasonic motor utilizing bulk lead zirconate titanate (PZT), Japanese journal of applied physics, Volume 38, pp.3347-3350.

[7] Morita T., Kurosawa M. K., and Higuchi T., 1998. A cylindrical micro ultrasonic motor using PZT thin film deposited by single process hydrothermal method (Φ 2.4 mm, L = 10 mm stator transducer), IEE transaction on ultrasonics, ferroelectrics and frequency control, Volume 45, No. 5, pp. 1178-1187.

[8] Morita T., Kurosawa M. K., and Higuchi T., 1996. Design of cylindrical ultrasonic micromotor to obtain mechanical output, Japanese journal of applied physics, Volume 35, pp.3251-3254.

[9] Morita T., Kurosawa M. K., and Higuchi T., 1995. An ultrasonic micromotor using a bending cylindrical transducer based on PZT thin film, Sensors and actuators A, Elsevier, Volume 50, pp. 75-80.

[10] Shukla R., Rajan K. K., Gandhi P., and Lim L. C., 2008. Complete sets of elastic, dielectric, and piezoelectric properties of [001]-poled Pb(Zn-1/3Nb2/3)O3 – (6-7)% PbTiO3 Single crystals of [110]-length cut, Applied Physics Letters 92, 212907 (2008).